agronomy

MDPI

Article

Study on the Natural Ventilation Characteristics of a Solar Greenhouse in a High-Altitude Area

Bohua Liang [1], Shumei Zhao [1], Yanfeng Li [2], Pingzhi Wang [1], Zhiwei Liu [3], Jingfu Zhang [1] and Tao Ding [1,*]

[1] College of Water Resources and Civil Engineering, China Agricultural University, Beijing 100080, China
[2] Tibet Academy of Agricultural and Animal Husbandry Sciences, Lhasa 851418, China
[3] Infrastructure Construction Department, China Agricultural University, Beijing 100080, China
* Correspondence: dingtao@cau.edu.cn

Abstract: The ventilation rate of a greenhouse is one of the major factors to consider when assessing its ventilation performance. Compared with plain areas, high-altitude areas have lower air pressure, thinner air, and stronger solar radiation, which in turn affect the magnitude of the local greenhouse ventilation rate. This paper is based on the use of online monitoring and computational fluid dynamics (CFD) techniques for modeling and model validation. The average relative error (ARE), mean absolute error (MAE), root-mean-square error (RMSE), and determination coefficient (R^2) of the temperature were 4.88%, 1.396 °C, 1.428 °C, and 0.9982, respectively. The ARE, MAE, RMSE, and R^2 of the velocity were 9.525%, 0.035 m/s, 0.049 m/s, and 0.9869, respectively. Then, the distributions of the wind pressure, Reynolds number (Re), thermal pressure, air density, air speed, and temperature in greenhouses in high-altitude and plain areas were researched to obtain the relevant factors affecting the ventilation rates of greenhouses in high-altitude areas. In addition, correlation analyses were conducted for five variables affecting the ventilation rate: the inlet velocity, the temperature difference between the inside and outside of the greenhouse, the air density difference between the inside and outside of the greenhouse, total indoor radiation, and the internal heat source of the crop, and the coefficients of their correlations with the greenhouse ventilation rate were 1.0, −0.83, −0.72, −0.72, and 0.68, respectively. A natural ventilation rate model for plateau areas was developed, with the ARE, RMSE, and R^2 between the sample values and fitted values determined to be 4.55%, 0.543 m^3/s, and 0.9997, respectively. The model was validated by predicting the greenhouse ventilation rate in winter (3 January 2022), and the ARE, RMSE, and R^2 of the sample values and predicted values were 9.726%, 8.435 m^3/s, and 0.9901, respectively. This study provides a theoretical basis for further research on greenhouse ventilation characteristics in high-altitude areas.

Keywords: high altitude; CFD simulation; wind pressure; thermal pressure; ventilation rate

Citation: Liang, B.; Zhao, S.; Li, Y.; Wang, P.; Liu, Z.; Zhang, J.; Ding, T. Study on the Natural Ventilation Characteristics of a Solar Greenhouse in a High-Altitude Area. *Agronomy* **2022**, *12*, 2387. https://doi.org/10.3390/agronomy12102387

Academic Editor: Francisco Manzano Agugliaro

Received: 24 August 2022
Accepted: 29 September 2022
Published: 2 October 2022

1. Introduction

Generally, high-altitude areas are defined as altitudes that exceed 2400 m. In China, altitudes of 2000–3000 m are about 7%, and those above 3000 m are about 25.9%. It is of great significance to develop facilities for the vegetable industry that can meet the demand of urban and rural residents in high-altitude areas and alleviate the problem of difficult-to-eat vegetables in high-altitude and marginal areas [1]. Compared with plain areas, high-altitude areas have stronger solar radiation, a larger temperature difference between day and night, and a thinner atmosphere with a lower density. Therefore, there are variations in the natural ventilation characteristics and ventilation rates of greenhouses.

In recent years, scholars at home and abroad have gradually conducted relevant studies on high-altitude areas. A. Agarwal et al. [2] studied the effect of plant density on the production of bell pepper in greenhouses in alpine and high-altitude areas, obtaining the optimal range of planting density. S. Acharya et al. [3] studied the effect of different organic fertilizers on the yield of garlic under greenhouse conditions in extreme winters,

which can be applied to be extended in the fragile ecosystem of the cold arid desert of the Ladakh region. Y. Chun et al. [4] studied the effects of plant morphological, physiological, and biochemical traits of *Populus przewalskii* in lower- and higher-altitude areas under water stress in a greenhouse, which revealed more protective mechanisms for *Populus przewalskii* in higher-altitude areas. R. Fuller et al. [5]. constructed a simple greenhouse in a remote local high-altitude area of Nepal and evaluated the thermal performance of the greenhouse. Simulations were conducted to propose improvements to the building enclosure and predict the impact of adding nighttime heat from an internal passive solar water collector. These research methods and ideas guided the study in this paper.

Scholars have researched greenhouse ventilation, including forced ventilation [6,7] and natural ventilation [8,9]. The former mainly relies on wet curtains and fans for ventilating and cooling, which is more flexible in terms of regulation measures to adjust the environmental climate in greenhouses. However, it needs to consume more energy and cannot contribute to sustainable development [10]. Natural ventilation is defined as the flow of indoor and outdoor air across the greenhouse window caused by the action of wind and thermal pressures. It is widely used in solar greenhouses and consumes little electric energy. Research has shown that thermal pressure dominates ventilation when the external wind speed is less than 0.5 m/s. When the external wind speed is higher than 1.5 m/s, the wind pressure dominates the ventilation. Wind pressure and thermal pressure combined dominate the ventilation for velocities between 0.5 m/s and 1.5 m/s [11]. In addition, the chimney effect provides effective thermal pressure ventilation [12–14]. In 1989, L. Okushima et al. [15] started to apply CFD techniques in greenhouses. This technique enabled a briefer analysis of the natural ventilation effect. Subsequently, CFD calculation algorithms were improved to make the results more accurate [16,17]. Meanwhile, scholars in this domain at home and abroad have numerically simulated the hydrothermal environment in solar and glass greenhouses [18,19]. J. Roy et al. [20] studied temperature and humidity in a semi-closed greenhouse based on CFD and conducted a sensitivity study on the effect of an air-conditioning device. T. Boulard et al. [21,22] used CFD to predict the transfer of fungal spores in a rose greenhouse and also studied the microclimate, canopy transpiration, and photosynthesis in greenhouses. M. Akrami et al. [23] researched the structural effects of single-span greenhouse vents at lower wind velocities by CFD and determined that the environmental effects of roof vents on the plant zone were minor. S. Hong et al. [24] calculated the greenhouse ventilation rate by CFD and tracer particles. L. He et al. [25] analyzed and discussed factors such as the air age, flow field distribution, and angles of the optimum air inlet and outlet inside the greenhouse based on CFD and entropy weight analysis. Thus, it is evident that the application of CFD in greenhouse ventilation is mainly focused on the analysis of the flow and temperature fields inside the greenhouse, as well as other related factors. Research on the criteria for wind pressure, thermal pressure, and Re for the ventilation flow pattern is scarce. Therefore, it is feasible to study the characteristic distributions of wind and thermal pressures in greenhouses by CFD.

The greenhouse ventilation rate is a major indicator of the greenhouse ventilation capacity, which can considerably affect the microclimate environment distribution in greenhouses [26]. Relevant scholars at home and abroad have conducted a lot of research on the greenhouse ventilation rate. Some scholars divided the ventilation rate of the greenhouse into the wind pressure ventilation rate and thermal pressure ventilation rate. According to different types of greenhouses, the relationships between the wind pressure ventilation rate, thermal pressure ventilation rate, and total ventilation rate have been researched. T. Boulard et al. [27] established a model of the ventilation rate for continuous roof vents. Through experimental tests and calculations, the wind pressure ventilation rate, thermal pressure ventilation rate, and total ventilation rate of double-side ventilation and single-side ventilation of greenhouses have been researched, with corrections applied for ventilation coefficients. F. Baptista et al. [28] investigated the wind pressure ventilation rate, thermal pressure ventilation rate, and total ventilation rate using tracer gas. Moreover, the

functional relationship between the three was researched to simplify the ventilation rate calculation formula. Then, F. Fang et al. [29] used carbon dioxide tracer gas to research the wind pressure and thermal pressure ventilation rates based on top-ventilated greenhouses. Equations from previous research were also combined to correct and fit the wind pressure–volume coefficients. A great number of scholars have conducted experiments and derived the ventilation rate calculation equation. C. Kittas et al. [30] combined previous experimental research and theoretical calculations to derive equations for the ventilation rate calculation. However, the format is relatively complex, and the measurement and collection of data are difficult. L. Wang et al. [31] researched meteorological data to acquire estimates of ventilation rates in different environments. Meanwhile, the correction coefficients for the heat area in different environments have been determined, and the ventilation rate equation has been derived theoretically by scholars. M. Sherman et al. [32] based the ventilation rate calculation on the Bernoulli equation of fluid mechanics. J. Fernandez et al. [33] solved the coefficients of this equation in their study by adjusting the opening of vents. The ventilation rate can be calculated by correcting the equation using the inlet velocity and the temperature difference between the inside and outside. This method reasonably simplifies the calculation. However, the determination of the ventilation rate correlation coefficients still requires extensive field experimental fitting and validation.

In this research, field experiments were conducted at high altitude, and a remote transmission platform was created for data collection. The distributions of wind and thermal pressure characteristics in a low-pressure environment were researched using the CFD technique, and the results were analyzed by comparing them with those in the plain area (altitude of 43.5 m in Beijing). Meanwhile, the ventilation rates under different operating conditions were calculated separately, and a correlation analysis and significance test of the influencing factors were performed. Finally, the ventilation rate of the solar greenhouse at high altitude was calculated and verified by combining the test data. This study not only provides a new idea for studying the ventilation characteristics of solar greenhouses in high-altitude areas but also greatly simplifies the calculation of the greenhouse ventilation rate in Lhasa, Tibet.

2. Materials and Methods

2.1. Experimental Site and Materials

The experimental solar greenhouse is located in the Tibetan Academy of Agricultural and Animal Husbandry Sciences, Lhasa (91.03° N, 29.64° E, altitude 3650 m). The greenhouse is oriented east to west, with a total area of 412 square meters, a span of 7.3 m, a length of 56.43 m, a height of 3.2 m, and a back wall height of 2.62 m. The greenhouse back wall is constructed of concrete and covered with plastic panels and insulation wool, while the film consists of PVC plastic. During this experiment, tomato crops were grown in the greenhouse, where plants were about 2 m high. The side vents were closed on rainy days. The top vents were covered with insulation cotton in winter when the temperature was low. The inlet of this greenhouse is situated on the south side, and the position of the inlet is 1.25 m from the ground, the height of the opening is 0.45 m, and the width of the opening is 0.4 m. The air outlet is located 1.2 m from the back wall, and the outlet is nearly horizontal with an opening of 0.4 m. The greenhouse cross-section is shown in Figure 1.

Outdoor environmental data were collected by Kunlun Coast's all-in-one weather station (weather station model: QXZM-M1). The relevant collected data include wind speed, wind direction, ambient temperature and humidity, radiation, and a series of other environmental climate variables, which were collected automatically every 30 min. The interior of the solar greenhouse uses side vents combined with top vents for ventilation regulation. Different types of sensors were arranged at different locations of the air vents and inside the greenhouse. The specifications of the greenhouse sensors are shown in Table 1.

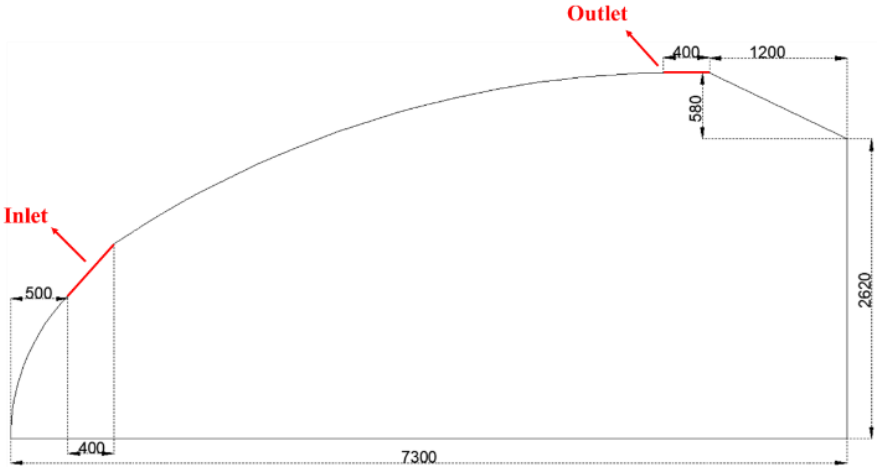

Figure 1. Greenhouse cross-section diagram.

Table 1. Sensor Specifications.

Instrument	Measurement Data	Measurement Range	Precision
PT100	Temperature	−40 °C~80 °C	±0.2 °C
Humidity sensor	Humidity	0 RH~99% RH	±3% RH (5% RH~95% RH, 25 °C)
Thermal bulb wind speed sensor	Velocity	0~5 m/s	±(0.03 m/s + 2% reading)
Light sensor	Total indoor radiation	0~2000 W/m^2	±10 W/m^2

For the purpose of comprehensively determining the distributions and change patterns of the temperature, humidity, velocity, and other environmental variables in the greenhouse over time and space, different types of sensors were arranged in the greenhouse. The horizontal direction is mainly arranged horizontally, while the vertical direction is mainly arranged in three layers to monitor the environmental changes at different heights. The sensor measurement points were arranged as in Figure 2.

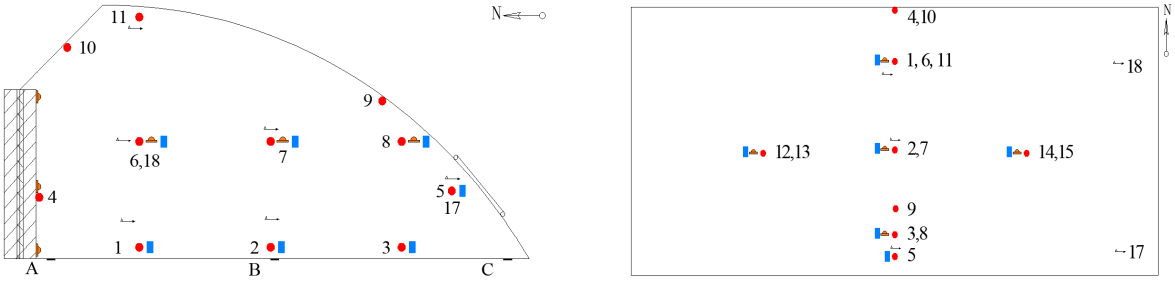

Figure 2. Locations of temperature sensors in the greenhouse: (**a**) side view; (**b**) overhead view.

The extraction of data was performed through a cloud platform, and then the obtained data were processed. The transmission platform is schematically shown in Figure 3.

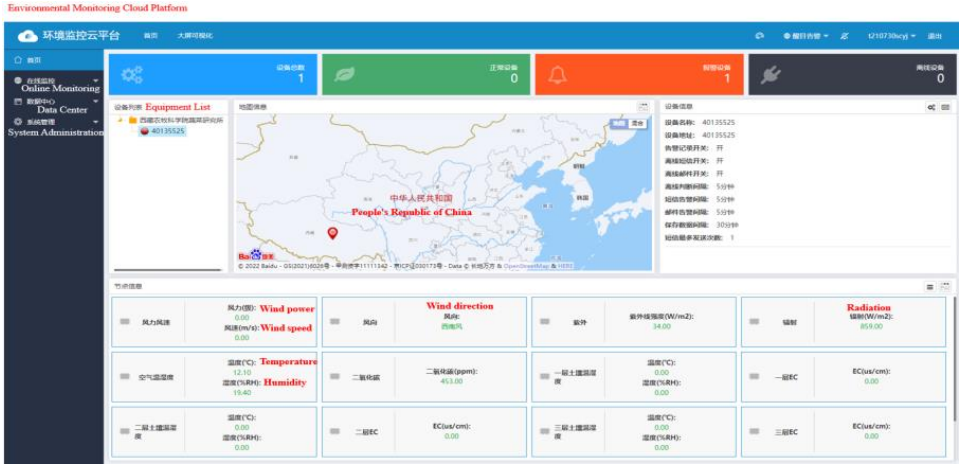

(**a**)

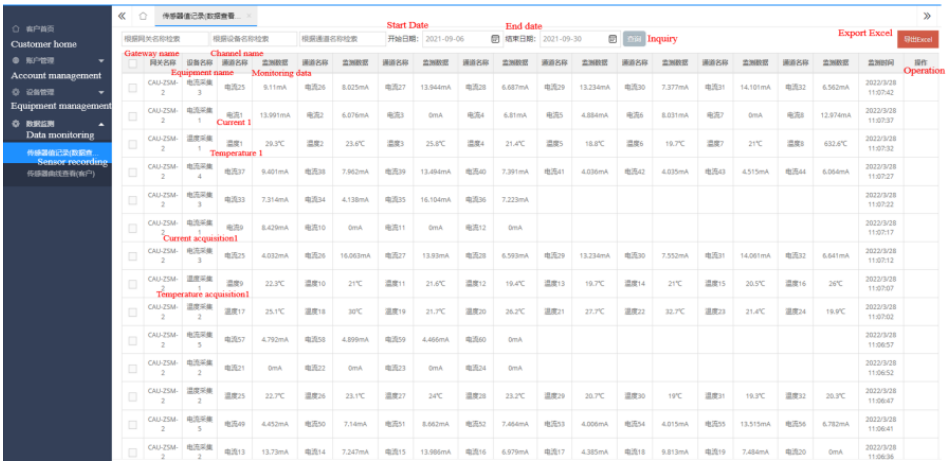

(**b**)

Figure 3. Internet-of-things transmission platform. (**a**) Platform of weather station. (**b**) Interior Sensor Platform.

2.2. CFD Model

The experimental greenhouse was numerically modeled and calculated by the CFD technique in this research. In the greenhouse, the airflow is slow, and the temperature change is minor, which is consistent with the Boussinesq hypothesis [10,34]. Thus, the state of airflow within the temperature chamber is considered incompressible turbulent flow. This model is discretized using the finite volume method and SIMPLEC algorithm. The basic control equation is Equation (1).

$$\frac{\partial(\rho\varphi)}{\partial t} + div(\rho u\varphi) = div(\Gamma grad\varphi) + S \tag{1}$$

In this case, φ is a generic variable that represents the solution variables, such as u, v, w, and T; Γ is the generalized diffusion coefficient; ρ is the air density, kg/m^3; u is the air velocity, m/s; and S is the generalized source term.

The researched greenhouse is located in Tibet, where the solar radiation is intensive in the noon hour of autumn and has a great influence on the flow field inside the greenhouse. Thus, in the CFD model, the solar radiation model (DO) is loaded by the sun-ray-tracing

method. In addition, the DO radiation model was chosen to consider the effect of thermal radiation. The radiation solution equation is Equation (2) [35].

$$\nabla \cdot \left(I\left(\vec{r}, \vec{s}\right)\vec{s} \right) + (a+\sigma_s) I\left(\vec{r}, \vec{s}\right) = an^2 \frac{\sigma T^4}{\pi} + \frac{\sigma_s}{4\pi} \Phi I\left(\vec{s}, \vec{s'}\right) d\Omega' \tag{2}$$

In this equation, $\vec{r}$ is the position vector; s is the along-range length; a is the absorption coefficient; n is the discount factor; σ_s is the scattering coefficient; σ is the Stefan–Boltzmann constant, with a value of 5.26×10^{-8} W/m^{2}K^4; I is the radiation intensity; T is the local temperature (K); Φ is the phase function; and Ω' is the spatial stereo angle.

To describe the tomato plants in the greenhouse in a porous medium, a source term is added to the momentum equation according to the Darcy–Forchheimer law. The porous medium is calculated as in Equation (3) [10,34,36].

$$S_u = \left(-\frac{\mu}{\alpha} u \right) + \left(-C_u \cdot \frac{1}{2} \rho |u| u \right) = \left(-D_u \mu u \right) + \left(-C_u \cdot \frac{1}{2} \rho |u| u \right) \tag{3}$$

In this case, S_u is the source term of the momentum equation; μ is the dynamic viscosity, m^2/s; α is the permeability of the porous medium, m^2; D_u is the viscous drag coefficient; and C_u is the inertia drag coefficient.

The sensible heat exchange between the crop canopy and the room air, the latent heat of transpiration of the crop, is calculated using the following equation. Finally, it is added to the energy equation in the form of a source term. The source of internal heat is calculated as in Equation (4) [10,37].

$$S_\Phi = 2LAI\rho C_p \frac{T_c - T_i}{r_a} + LAI\rho\lambda \frac{H_c - H_a}{r_a + r_s} \tag{4}$$

S_Φ is the source term of the energy equation; LAI is the leaf area index, m^2/m^2; T_c and T_i are the temperatures of the crop and the indoor air, K; r_a is the aerodynamic impedance of the crop boundary layer, s/m; λ is the latent heat of evaporation of water, J/kg; r_s is the average impedance of the crop stomata, s/m; and H_c and H_a are the relative humidity of the crop and the indoor air.

The aerodynamic impedance of the crop boundary layer and the average impedance of the crop porosity are calculated in Equations (5) and (6) [34].

$$r_a = \begin{cases} 840 \left(\frac{d}{|T_c - T_i|} \right)^{0.25} & u < 0.1\ m/s \\ 220 \left(\frac{d^{0.2}}{u^{0.8}} \right) & u < 0.1\ m/s \end{cases} \tag{5}$$

$$r_s = 200 \left(1 + \frac{1}{exp\left(0.05\left(R_{gi} - 50\right)\right)} \right) \cdot \left(1 + 0.11 exp\left(0.34 \frac{D_i}{100} - 10 \right) \right) \tag{6}$$

R_{gi} is the internal solar radiation; D_i is the saturated water vapor pressure difference; and d is the characteristic blade length per unit length. All parameters are added to the control equation in the form of source terms.

The Mach number is generally used to determine the compressibility of a fluid. When the number is less than 0.3, the fluid is considered incompressible, calculated as in Equation (7) [38].

$$M = \frac{u}{c} = \frac{u}{\sqrt{kRT}} \tag{7}$$

where c is the velocity of sound propagation within the fluid; R is the molar gas constant; and k is the isentropic index, which is calculated to be 1.4 for air [39]. From these calculations, M is 4.55×10^{-3} and 3.35×10^{-2} in the selected working conditions. Hence, because M is less than 0.3, the gas in the greenhouse can be considered an incompressible fluid.

The state of the flow of air is usually discriminated by Re, which reflects the relationship between the magnitude of the inertial and viscous forces. The calculation equation is shown in Equation (8) [40].

$$\mathrm{Re} = \frac{ul}{v} \tag{8}$$

where l is the characteristic length. In this research, Re is far more than 4000. The air in the greenhouse can be considered a low-velocity incompressible fluid with turbulent properties [38].

In general, the ratio of the total area of plant leaves to the land area is defined as the leaf area index (LAI). The calculation equation is shown in Equation (9) [41].

$$\mathrm{LAI} = \frac{\sum_1^n S_{leaf}}{S_{soil}} \tag{9}$$

where n is the number of leaves; S_{leaf} is the area of each leaf; and S_{soil} is the area covered by soil. In this study, we measured and obtained the average values for different types of leaves to obtain the value of the greenhouse LAI for this experiment.

2.3. Boundary Conditions and Geometric Modeling

CFD models using the RNG k-ε dual-square turbulence model were used with the standard wall function treatment in the near-wall region [42,43]. Under natural ventilation conditions, the inlet velocity and outlet pressure were used as boundary conditions. The major boundary conditions, such as the temperatures of the air inlet and outlet, the wind velocity of the air inlet, and the solar radiation within the room, were further calculated based on the data transmitted remotely from the sensors. Taking the indoor reference temperature as an example, the calculated value can be obtained by selecting the temperature data from four indoor monitoring points (monitoring point 1, monitoring point 2, monitoring point 6, and monitoring point 7) and taking their average values. The wind velocity of the inlet was obtained by averaging the data from measurement point 5 and measurement point 17, while the temperature of the outlet was determined from the data collected at measurement point 11 (the monitoring points are distributed as in Figure 2).

In the crop section, the associated physical parameters of the plants were collected through field tests. The temperature and humidity of the plant leaves were measured with a chlorophyll meter, the humidity and atmospheric pressure around the plants were measured with a thermal anemometer, the breeze speed around the plants was measured with a thermal anemometer, and the dimensions of the leaves were measured with a micrometer and vernier calipers, which led to the calculation of the LAI. Finally, the evapotranspiration of the plant was calculated from the measured data and then assigned to the CFD model in the form of an endothermic source for calculations.

In the process of CFD model construction, the physical parameters of the wall, as well as the soil and other materials, are involved. Considering the financial cost, the density, specific heat, and thermal conductivity of these materials were obtained from the literature to obtain the specific values of these parameters. This calculation was carried out for the solar greenhouse based on its equilibrium state. Therefore, we consider parameters such as light conditions and boundary conditions to be equilibrium values. The specific parameter settings are shown in Table 2.

According to the size of the greenhouse measurements, 3D modeling was performed. To conveniently facilitate subsequent calculations, the simplified model of the heliostat was developed with a structured mesh, with a total mesh of 2.39 million and good quality. The model is displayed in Figure 4.

Table 2. Basic parameters and boundary condition settings.

Parameters	Boundary Conditions	Parameters	Boundary Conditions
Air Density (kg/m^3)	0.761	Pressure (Kpa)	66.1
Air thermal conductivity (W·m^{-1}·K^{-1})	0.027	Wall temperature (°C)	23.8
Viscosity (m^2/s)	2.63×10^{-5}	Inlet velocity (m/s)	0.27
Specific heat of air (J·kg^{-1}·K^{-1})	1005.93	Inlet temperature (°C)	30.5
Wall density (kg/m^3)	1600	Outlet temperature (°C)	28.5
Specific heat of the wall (J·kg^{-1}·K^{-1})	1051	Crop temperature (°C)	27.3
Thermal conductivity of walls (W·m^{-1}·K^{-1})	0.76	Covering film temperature (°C)	47.0
Soil density (kg/m^3)	1700	Soil temperature (°C)	27.5
Soil specific heat (J·kg^{-1}·K^{-1})	1010	Crop canopy pressure drop coefficient (°C) [10,34]	0.395
Soil thermal conductivity (W·m^{-1}·K^{-1})	0.8	Internal dropout factor (C_1) [10,34]	0.2
Covering film density (kg/m^3)	950	Crop porosity	0.7
Covering film specific heat (J·kg^{-1}·K^{-1})	1600	leaf area index (LAI)	2.6
Thermal conductivity of covering film (W·m^{-1}·K^{-1})	0.29	Latent heat of evaporation (J·kg^{-1})	2.43
Crop density (kg/m^3)	560	Saturated water vapor pressure difference (Pa)	650
Crop specific heat (J·kg^{-1}·K^{-1})	2100	d (mm)	6.0
Crop thermal conductivity (W·m^{-1}·K^{-1})	0.19	r_a (s·m^{-1})	225.4
Indoor radiation (W/m^2)	743	r_s (s·m^{-1})	200
Air temperature (°C)	29.55	Internal heat source (W/m^3)	19.96

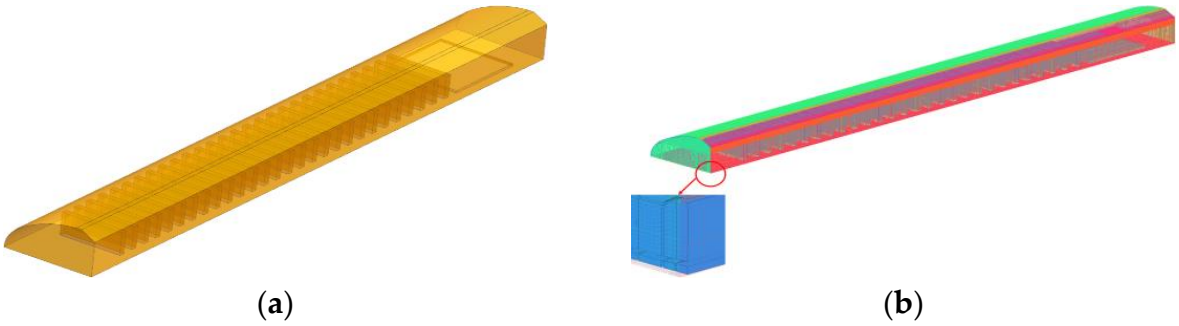

Figure 4. Greenhouse model. (**a**) Three-dimensional model. (**b**) Structured grids.

In this paper, CFD calculations, the spatial discretizations of the gradient, pressure, momentum, turbulent kinetic energy, turbulent dissipation rate, energy, and discrete ordinates are least-squares-call-based, second-order, second-order upwind, first-order upwind, first-order upwind, second-order upwind, and first-order upwind, respectively. The scheme of the algorithm is SIMPLEC, and the skewness correction is zero. In addition, the residuals of continuity, x-velocity, y-velocity, z-velocity, energy, k, epsilon, and DO intensity are 10^{-3}, 10^{-3}, 10^{-3}, 10^{-3}, 10^{-6}, 10^{-3}, 10^{-3}, and 10^{-6}, respectively.

2.4. Grid Irrelevance Verification

The numerical simulation of the transients requires the verification that the selected number of meshes is irrelevant to the corresponding computational results, which means validating the grid independence of the created model. CFD models with six different grid numbers were created: 0.71 million, 1.21 million, 1.69 million, 2.39 million, 3.48 million, and 4.2 million grids. The calculated and tested temperature values for different monitoring points (Figure 2) are shown in Figure 5a; the calculated and tested wind speed values are shown in Figure 5b. When the number of grid cells exceeds 2.39 million, the error in the temperature calculation decreases to 4.88%, and the error in the wind speed calculation decreases to 9.49%. The calculation accuracy improves slightly as the number of grids continues to increase. Combining the calculation of accuracy and efficiency, 2.39 million grids were used for the subsequent calculation.

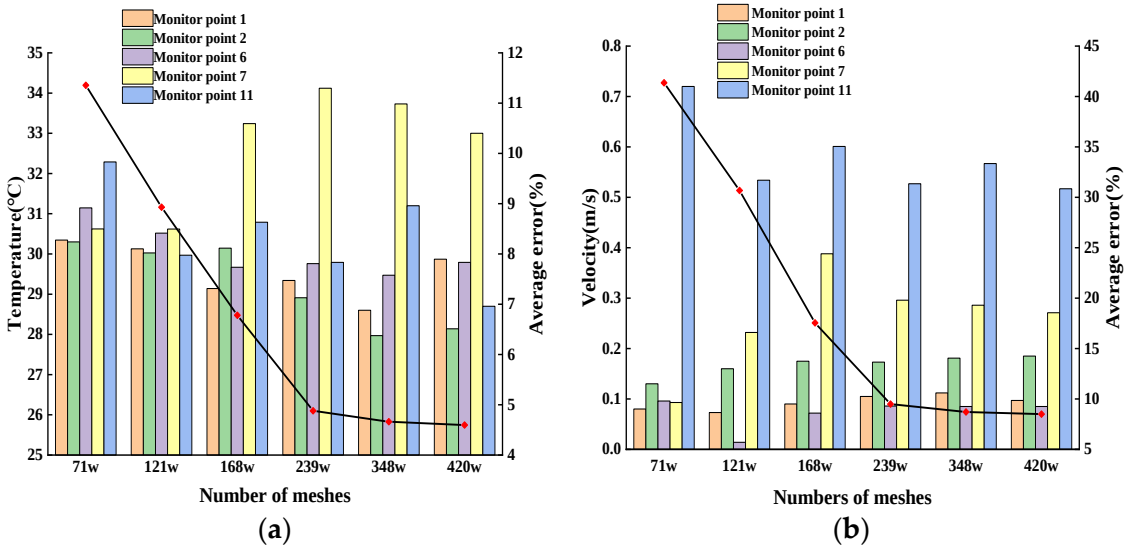

Figure 5. Grid independence verification. (**a**) Temperature verification. (**b**) Wind speed verification.

2.5. CFD Model Validation

To validate the accuracy and reliability of the CFD model, the measured values in the canopy area were compared with the calculated values, and the results are displayed in Figure 6.

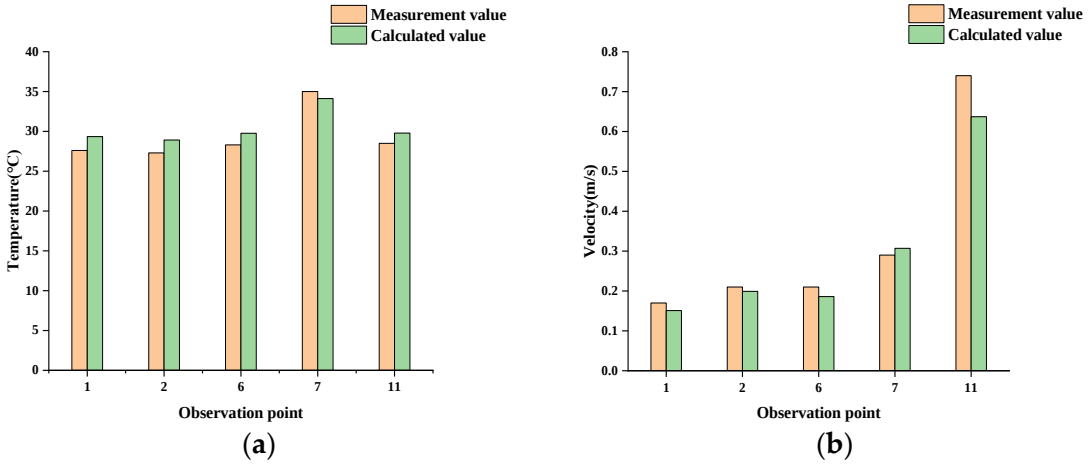

Figure 6. Validation of calculated and measured values. (**a**) Temperature validation. (**b**) Velocity validation.

From the calculations, the ARE, MAE, RMSE, and R^2 are displayed in Table 3.

Table 3. CFD Validation.

Observation Point	Temperature (°C)		Velocity (m/s)	
	Measurement Value	Calculated Value	Measurement Value	Calculated Value
1	27.6	29.34	0.17	0.151
2	27.3	28.91	0.21	0.199
6	28.3	29.76	0.21	0.186
7	35	34.12	0.29	0.307
11	28.5	29.79	0.74	0.637
ARE	-	4.880%	-	9.525%
MAE	-	1.396	-	0.035
RMSE	-	1.428	-	0.049
R^2	-	0.9982	-	0.9869

Although there are some deviations between the CFD calculation results and experimental test data, the distributions of the temperature and flow field, as well as the overall trend of change, are relatively consistent. This result indicates that the CFD model is valid and accurate and can be used for further calculations.

3. Results and Discussion

3.1. Wind and Heat Pressure Calculations

The distributions of wind and thermal pressures in the greenhouse in the high-altitude area are analyzed and discussed based on the CFD model. According to the test data and literature research, two computational conditions were added. The calculated results of three working conditions were used to study the wind pressure, thermal pressure, and coupled ventilation effects with different inlet air velocities. The main boundary conditions are listed in Table 4.

Table 4. Main calculation boundaries.

Inlet Velocity (m/s)	Reference Temperature (°C)	Reference Pressure (Pa)	Inlet Temperature (°C)	Outlet Temperature (°C)
1.95	17.30	66,780	19.0	18.1
0.27	29.55	66,100	30.5	28.5
1.3	23	66,340	24	23.8

The ventilation driven by wind pressure is mainly caused by the wind speed of the inlet of the greenhouse. Assuming that the wind speed near the air inlet is constant, the wind pressure calculation equation is obtained as follows:

$$\Delta P_w = 1/2 C_w \rho u^2 \tag{10}$$

ΔP_w is the pressure difference between inside and outside at the greenhouse vent caused by the outdoor wind speed, Pa; C_w is the wind pressure coefficient of volume.

Ventilation driven by thermal pressure is mainly caused by the density difference at different levels, which is associated with the temperature variation at different height locations. The equation for calculating the thermal pressure is as follows [29]:

$$\Delta P_s = \Delta P_0 - \rho g \left(\frac{\Delta T}{T} \right) y \tag{11}$$

ΔP_s is the pressure difference inside and outside the greenhouse vent caused by the thermal pressure, Pa; ΔP_0 is the reference pressure; and y is the vertical distance from a point in the greenhouse to the floor.

There are two sections of the solar greenhouse selected separately for the study, where x = 4000 mm is the crop section and x = 600 mm is the non-crop section, as shown in Figure 7.

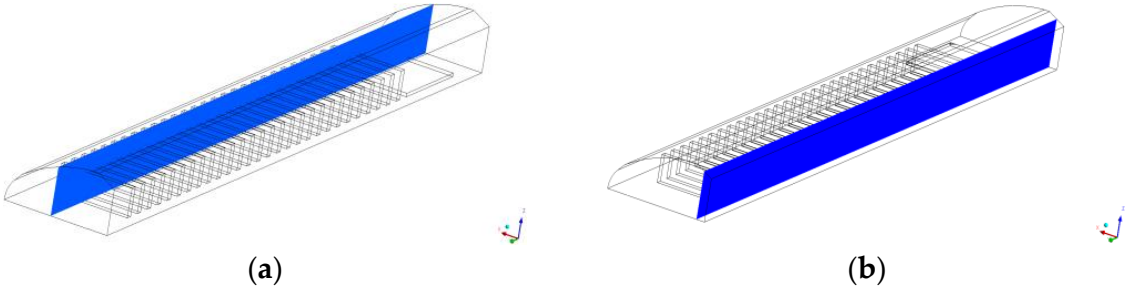

(**a**) (**b**)

Figure 7. Solar greenhouse study cross-section: (**a**) x = 4000 mm (crop area); (**b**) x = 600 mm (non-crop area).

3.1.1. Wind Pressure Ventilation

In the morning, at 10:00 am, with the inlet velocity u = 1.95 m/s, the airflow is mainly affected by the wind pressure, with the research mainly focused on the air convection caused by the wind pressure. The calculation results are displayed in Figure 8. Meanwhile, after adjusting the DO radiation model, heat source within the plant, air density, and reference atmospheric pressure, the wind pressure distribution characteristics in the plain area (the altitude is 43.5 m in Beijing) are shown in Figure 9.

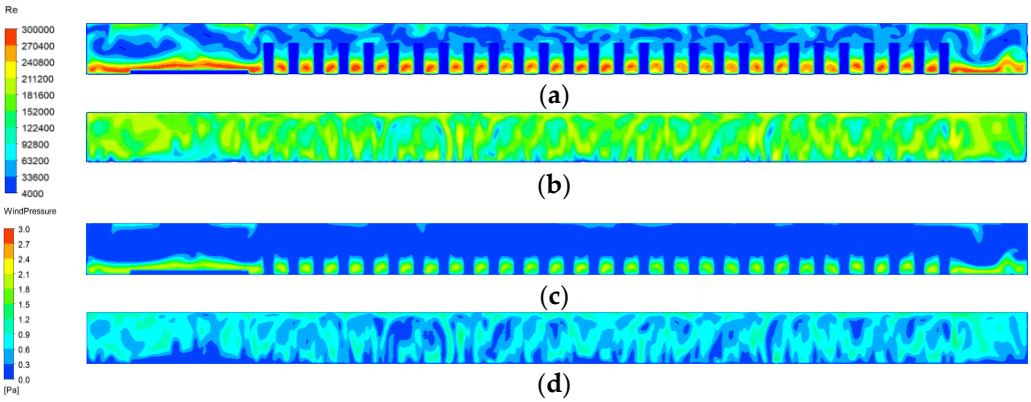

Figure 8. Wind pressure ventilation characteristics in the high-altitude area of: (**a**) x = 4000 mm, Re; (**b**) x = 600 mm, Re; (**c**) x = 4000 mm, wind pressure; (**d**) x = 600 mm, wind pressure.

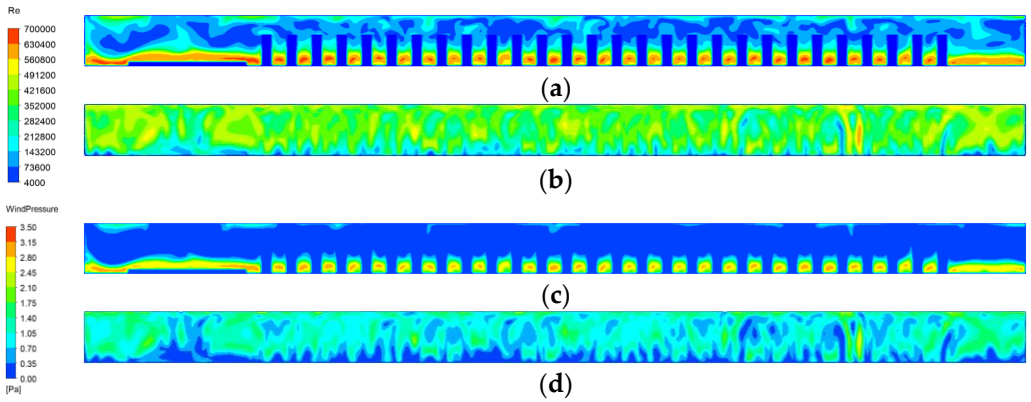

Figure 9. Wind pressure ventilation characteristics in the plain area of: (**a**) x = 4000 mm, Re; (**b**) x = 600 mm, Re; (**c**) x = 4000 mm, wind pressure; (**d**) x = 600 mm, wind pressure.

Figure 8a,c show the distributions of Re and wind pressure in the section where the crop is located. In this figure, Re and wind pressure are larger in the crop gap area, where Re exceeds 2.7×10^5 and wind pressure exceeds 1.2 Pa in the region near the ground, with a decreasing trend as the height rises. Similarly, Re exceeds 5.5×10^5 and wind pressure exceeds 2.8 Pa in the region close to the ground in the crop gap area, with a decreasing trend as the height rises, as displayed in Figure 9a,c.

Re and wind pressure in the non−crop section (Figure 8b,d and Figure 9b,d) are unevenly distributed and show extremely turbulent characteristics, with an overall increasing trend as the height impedance rises.

Further calculation results are displayed in Figure 10. The height of z = 1500 mm inside the greenhouse was selected, and the results were obtained by extracting the Re and wind pressure values at the cross−sections of x = 4000 mm (crop section) and x = 600 mm (non−crop section), respectively, along the length direction (y-direction) of the greenhouse. In the crop section, the Re in the high-altitude area is about 46.86% and the wind pressure is about 71.34% of those in the plain area; in the non−crop section, the Re and wind pressure in the high-altitude area are about 45.54% and 80.47% of those in the plain area.

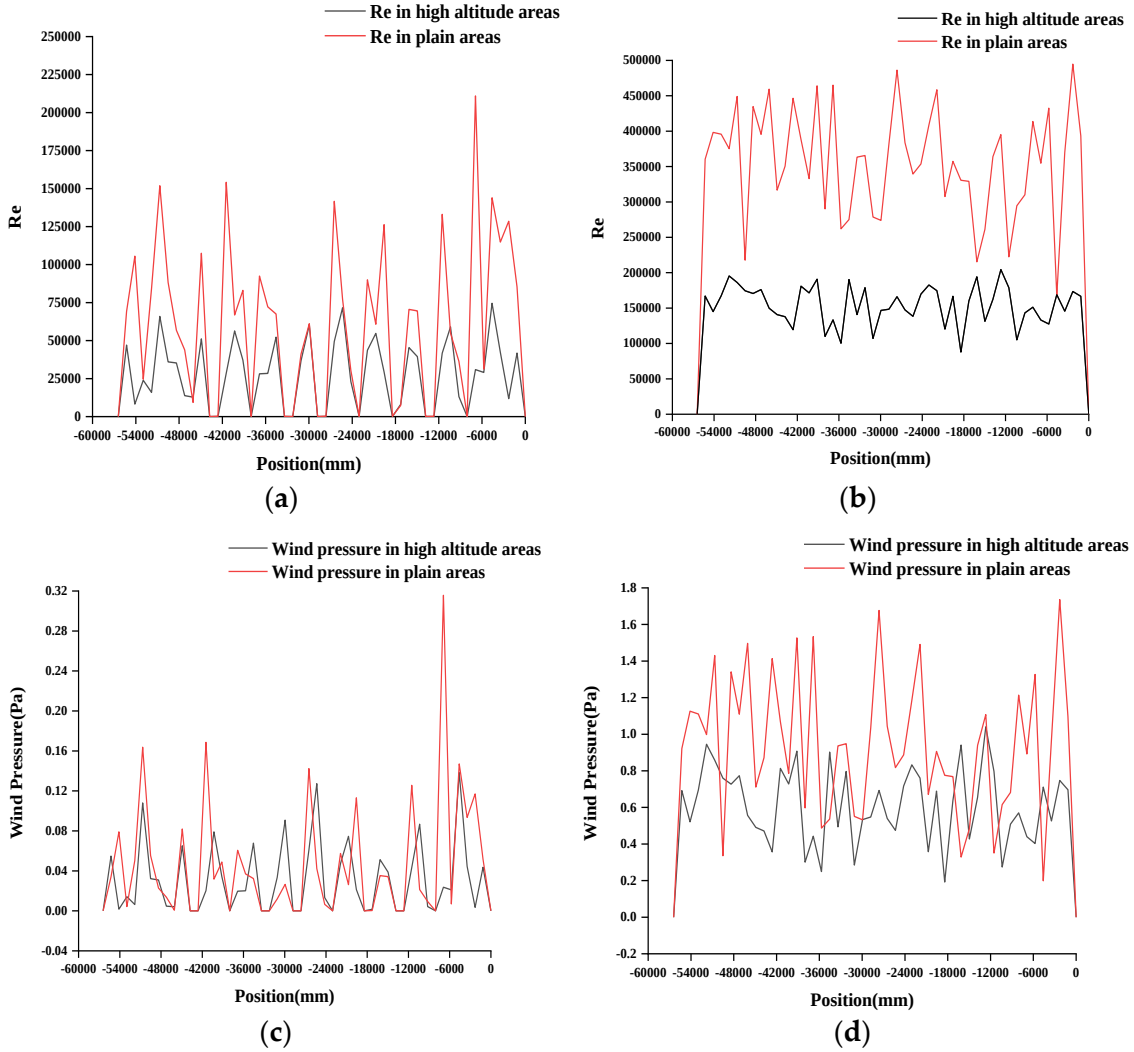

Figure 10. Variation in wind pressure characteristic parameters in high−altitude and plain areas of: (**a**) x = 4000 mm, Re; (**b**) x = 600 mm, Re; (**c**) x = 4000 mm, wind pressure; (**d**) x = 600 mm, wind pressure.

3.1.2. Thermal Pressure Ventilation

At 14:00 in the afternoon, with the inlet velocity u = 0.27 m/s, there is a significant temperature gradient in the greenhouse, and the ventilation is mainly thermal-pressure-driven at this time. The distributions of the thermal pressure and air density in high−altitude and plain areas are presented in Figures 11 and 12, respectively.

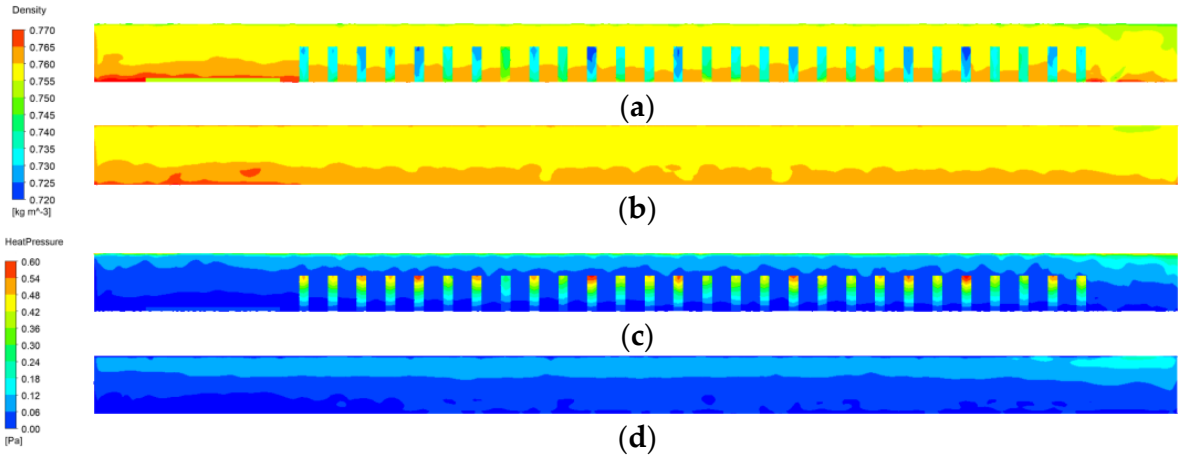

Figure 11. Thermal pressure ventilation characteristics in the high−altitude area of: (**a**) x = 4000 mm, density; (**b**) x = 600 mm, density; (**c**) x = 4000 mm, heat pressure; (**d**) x = 600 mm, heat pressure.

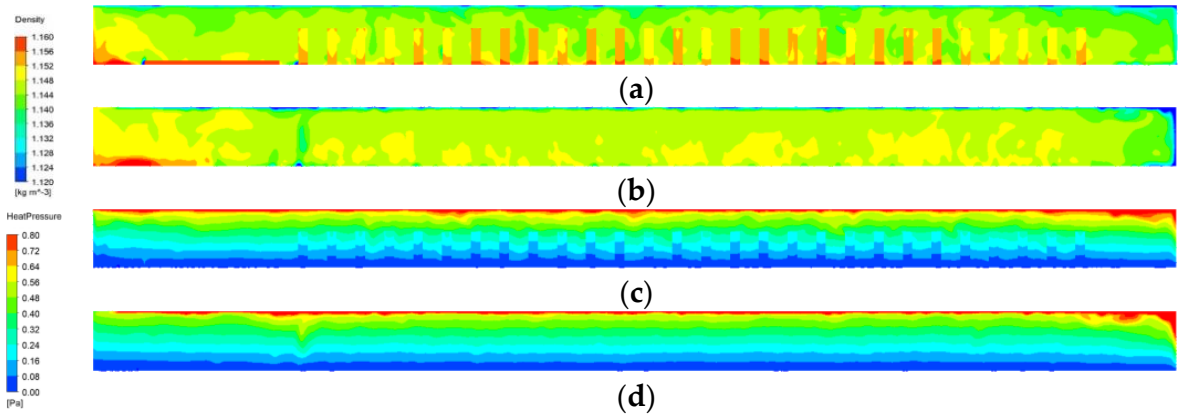

Figure 12. Thermal pressure ventilation characteristics in the plain area of: (**a**) x = 4000 mm, density; (**b**) x = 600 mm, density; (**c**) x = 4000 mm, heat pressure; (**d**) x = 600 mm, heat pressure.

In the crop area, the intense solar radiation and the evaporation and transpiration of crops in the plateau area lead to a density difference around the crop (0.03 kg/m^3), which is about 187.5% higher than that in the plain area (0.016 kg/m^3) (Figures 11a and 12a), and the thermal pressure in the crop canopy area (0.6 Pa) is about 250% higher than that in the plain area (0.24 Pa) (Figures 11c and 12c). In the non−crop area, the density decreases with height in the plateau area, and the thermal pressure reverses (Figure 11b,d); in the plain area, the thermal pressure distribution pattern is consistent with that in the plateau area, but the density distribution is more disordered, which indicates that the air density in the plain area is less variable.

Further calculation results are presented in Figure 13. The height of z = 1500 mm inside the greenhouse was selected, and the results were obtained by extracting the density and heat pressure values at the cross-sections of x = 4000 mm (crop section) and x = 600 mm (non−crop section) along the length direction (y−direction) of the greenhouse. The air density at high altitude is 66% of that in the plain area in both crop and non−crop areas, while the thermal pressure is 57.95% and 16.68% of that in the plain area, respectively.

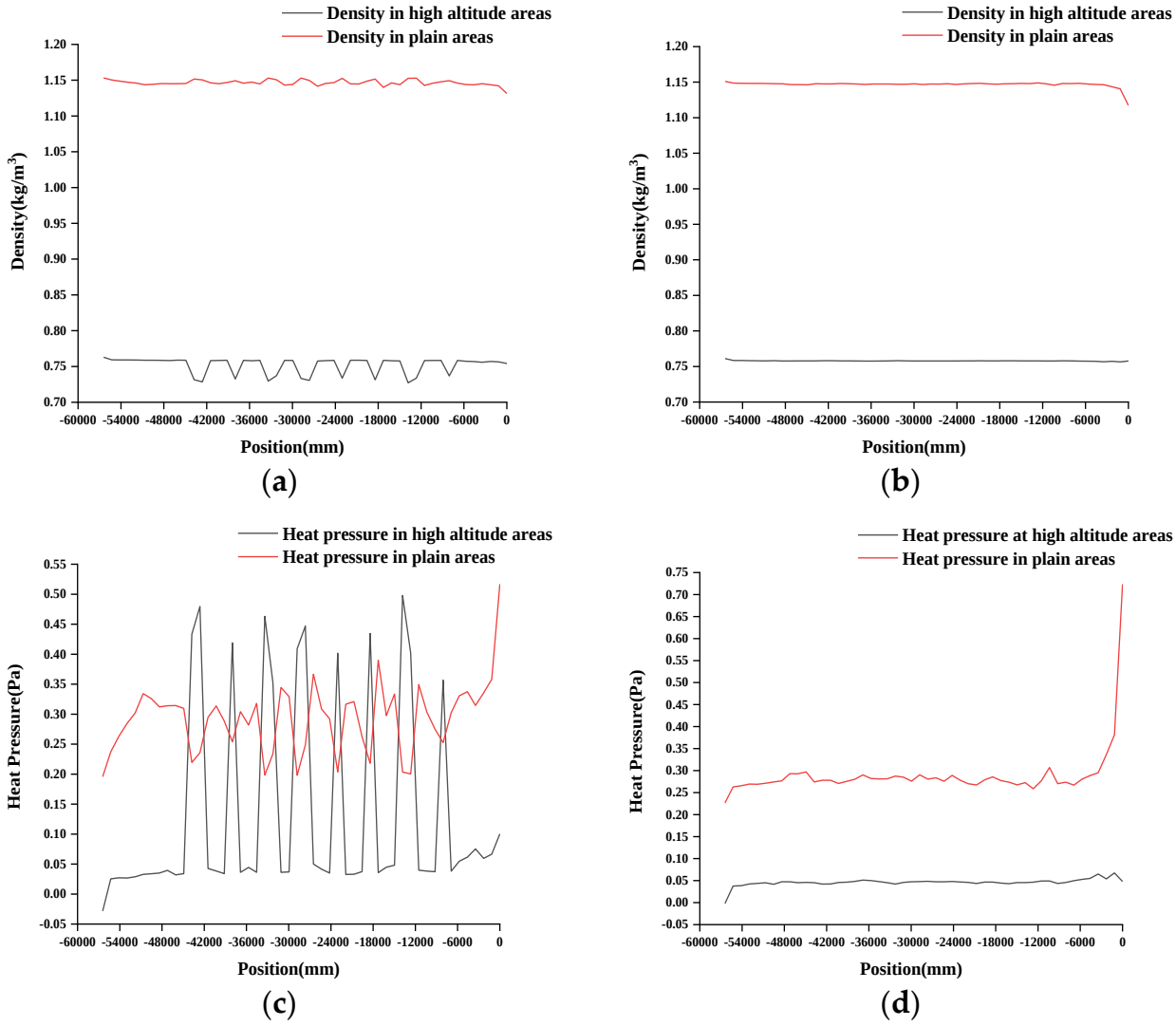

Figure 13. Variation in thermal pressure characteristic parameters in high−altitude and plain areas of: (**a**) x = 4000 mm, density; (**b**) x = 600 mm, density; (**c**) x = 4000 mm, heat pressure; (**d**) x = 600 mm, heat pressure.

3.1.3. Coupled Wind and Thermal Pressure Ventilation

At 18:00 pm, with the inlet velocity u = 1.3 m/s, the air in the greenhouse is driven by the coupling effect of wind and thermal pressure; hence, the convection and diffusion effects of air are comprehensively considered. The air speed and temperature distributions of coupled ventilation in high−altitude and plain areas are shown in Figures 14 and 15, respectively.

Compared with the plain area, in the late afternoon, the wind speed between the crops is higher, resulting in a strong heat exchange between the crops with the surrounding air. This makes the temperature around the plants higher compared to the surrounding air and plants (Figure 14a,c). In contrast, in the non−crop area, there is no significant pattern in the wind speed and temperature distributions (Figure 14b,d).

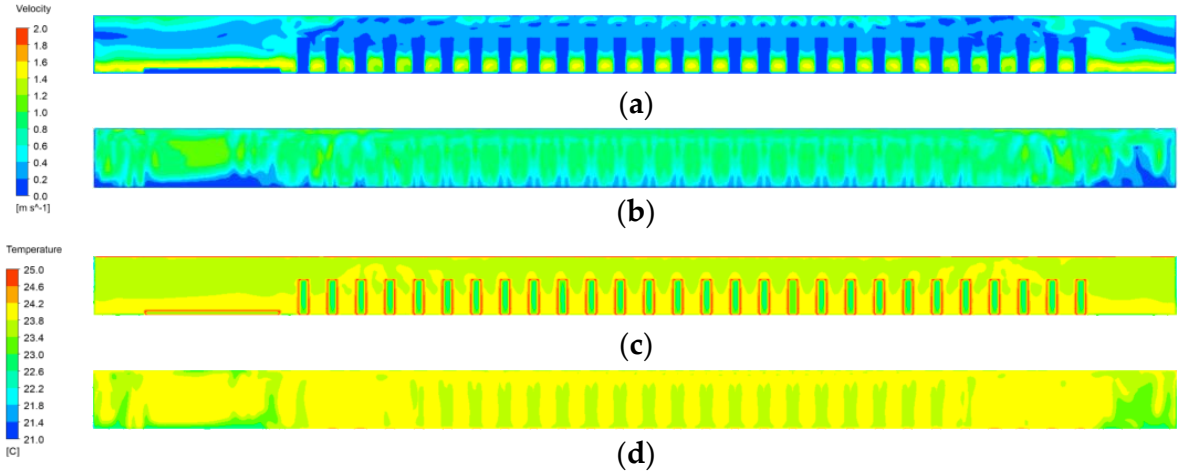

Figure 14. Coupling ventilation characteristics in the high−altitude area of: (**a**) x = 4000 mm, velocity; (**b**) x = 600 mm, velocity; (**c**) x = 4000 mm, temperature; (**d**) x = 600 mm, temperature.

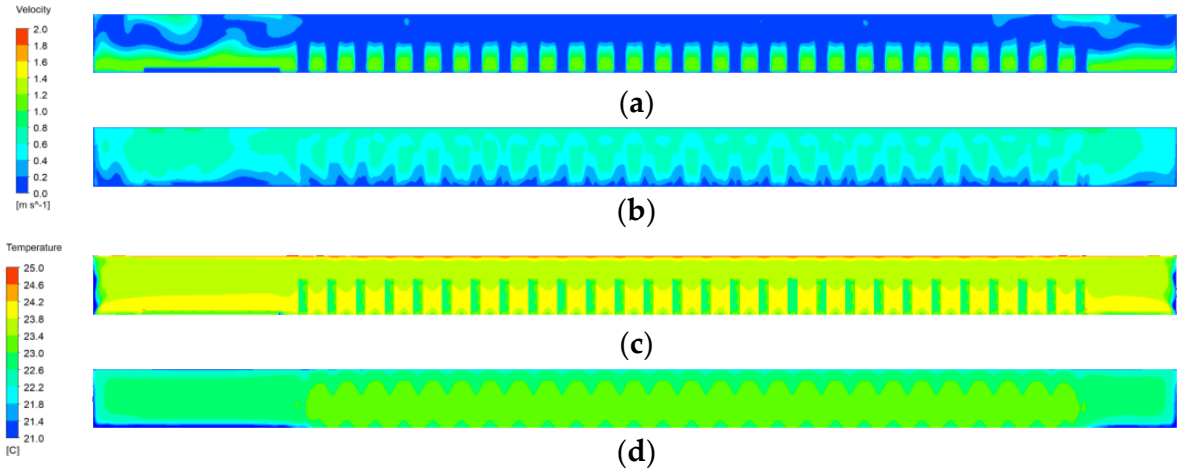

Figure 15. Coupled ventilation characteristics in the plain area of: (**a**) x = 4000 mm, velocity; (**b**) x = 600 mm, velocity; (**c**) x = 4000 mm, temperature; (**d**) x = 600 mm, temperature.

In the plain area, the higher air density and weaker solar radiation result in a lower wind speed between crops and less temperature variation with the surrounding air (Figure 15a,c). However, in the non−crop area, the distributions of air speed and temperature are different from those in the plain area, which affects the ventilation rate (Figure 15b,d).

Based on further calculations, as displayed in Figure 16, the height of z = 1500 mm inside the greenhouse was selected, and the results were obtained by extracting the velocity and temperature values at the cross−sections of x = 4000 mm (crop section) and x = 600 mm (non−crop section) along the length direction (y−direction) of the greenhouse. The temperature is larger in the crop and non−crop sections in the high−altitude area, which is 103% higher than that in the plain area, while the air speed distributions are 106% and 416%, respectively.

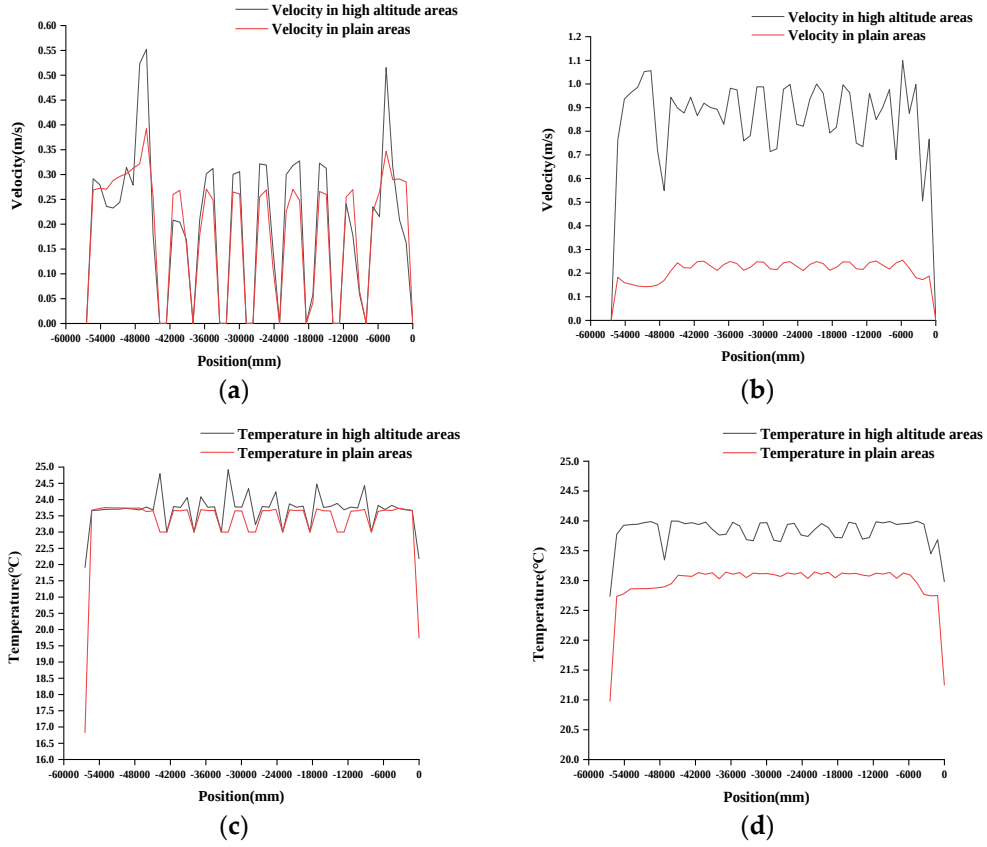

Figure 16. Variation in coupled ventilation parameters in high−altitude and plain areas of: (**a**) x = 4000 mm, velocity; (**b**) x = 600 mm, velocity; (**c**) x = 4000 mm, temperature; (**d**) x = 600 mm, temperature.

3.1.4. Discussion

CFD models were constructed from experimental measurements to obtain the calculation results for wind pressure ventilation, thermal pressure ventilation, and coupled ventilation. Meanwhile, the calculation results for the high-altitude area were compared with those of the plain area to draw the following conclusions.

In the morning (10:00 am), the wind velocity is higher (u = 1.95 m/s), and the wind pressure dominates the ventilation; in the afternoon (14:00 pm), the temperature is higher, and the wind velocity is lower (u = 0.27 m/s), with the thermal pressure dominating the ventilation; in the late afternoon (18:00 pm), the wind velocity decreases (u = 1.3 m/s), with the wind pressure and thermal pressure coupling ventilation dominating. Therefore, it can be known that the inlet velocity affects the ventilation rate. In the thermal pressure characteristics study, compared with the plain area, the high−altitude area had stronger solar radiation and thinner air, with the air density and thermal pressure being only 66% and 37.32% of those in the plain area. Thus, the difference in the air density between the inside and outside of the greenhouse, total radiation, and plant evaporation and transpiration will affect the ventilation rate. In the coupled ventilation study, compared with the plain area, the wind speed is higher in the high-altitude area, about 261% higher than that in the plain area, with a similar distribution pattern; the temperature is about 103% higher than that in the plain area, but there are large differences in its distribution. Therefore, the influence of the temperature difference between the inside and outside of the greenhouse on the greenhouse ventilation rate is further considered.

In conclusion, there are five relevant factors that affect the ventilation rate at high altitude: the inlet velocity, the temperature difference between the inside and outside of the greenhouse, the air density difference between the inside and outside of the greenhouse, total indoor radiation, and the internal heat source of the crop in the greenhouse.

3.2. Ventilation Rate

The greenhouse ventilation rate reflects the ventilation effect of the greenhouse during a period of time, which is a significant guideline for the ventilation control of the greenhouse. In the past, scholars who studied the greenhouse ventilation rate mainly focused on plain areas; therefore, the formula needs to be modified when calculating the greenhouse ventilation rate in a high-altitude area.

3.2.1. Sample Values of Greenhouse Ventilation Rate

The calculations were carried out by selecting ten sets of data for different working conditions. The boundary conditions for the calculations are displayed in Table 5.

Table 5. Boundary conditions for ventilation calculation.

Period	Reference Temperature (°C)	Velocity (m/s)	Inlet Temperature (°C)	Outlet Temperature (°C)
9:00	14.18	1.21	15.6	15.7
10:00	17.30	1.95	19.0	18.1
11:00	23.30	0.42	24.6	21.7
12:00	23.48	1.91	24.8	22.2
13:00	27.75	0.15	28.8	25.8
14:00	29.55	0.27	30.5	28.5
15:00	30.60	0.14	28.8	28.2
16:00	27.85	1.11	29.4	26.8
17:00	24.45	1.32	26.3	24.6
18:00	23	1.3	24	23.8

The sample values of the greenhouse ventilation rate were calculated based on the above boundary conditions, which are provided in Figure 17.

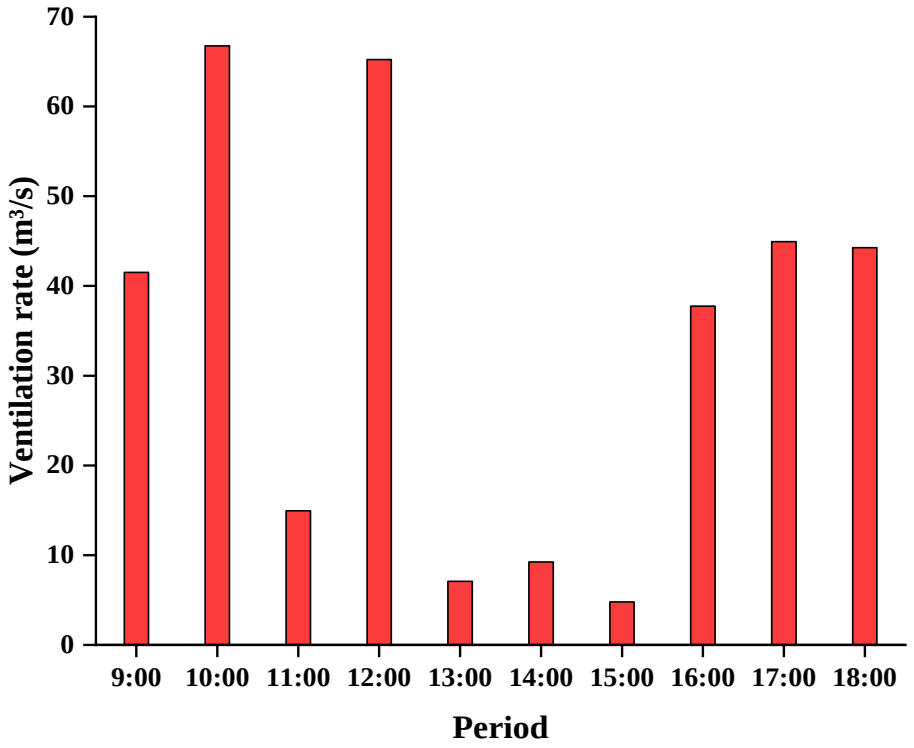

Figure 17. Sample values of greenhouse ventilation rate.

3.2.2. Correlation Analysis of Factors Affecting Ventilation Rate

The calculation results of the greenhouse ventilation rate, the inlet velocity, the temperature difference between the inside and outside of the greenhouse, the air density difference between the inside and outside of the greenhouse, total indoor radiation, and the internal heat source of the crop are shown in Table 6.

Table 6. Values calculated for ventilation−rate−related factors.

Period	Ventilation Rate (m^3/s)	Inlet Velocity (m/s)	ΔT (°C)	Δρ (kg/m^3)	Total Radiation (W/m^2)	Heat Source (W/m^3)
9:00	41.51	1.21	1.20	0.003	40	116.20
10:00	66.76	1.95	0.93	0.004	301	113.14
11:00	14.95	0.42	5.53	0.015	523	8.24
12:00	65.24	1.91	2.88	0.005	213	25.27
13:00	7.09	0.15	7.35	0.011	394	11.94
14:00	9.25	0.27	7.43	0.008	743	19.96
15:00	4.80	0.14	9.85	0.022	639	12.88
16:00	37.76	1.11	6.80	0.000	412	53.52
17:00	44.94	1.32	5.15	0.002	366	75.11
18:00	44.27	1.30	3.90	0.003	296	60.70

A correlation analysis and significance test were performed based on Origin for the ventilation rate's influencing factors, and the calculated results are presented in the form of heat maps, which are shown in Figure 18.

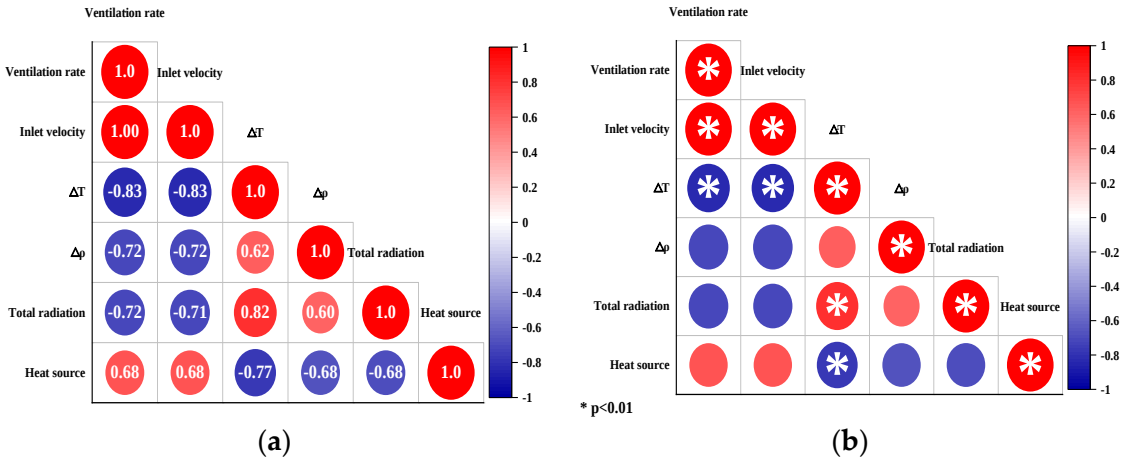

Figure 18. Ventilation rate correlation factor analysis. (**a**) Correlation coefficient calculation. (**b**) Significance analysis.

Figure 18a shows that the variables with absolute values of the correlation coefficient r exceeding 0.8 (extremely strong correlation) are the inlet velocity and the temperature difference between the inside and outside of the greenhouse, which indicates that they are both main influencing factors of the greenhouse ventilation rate. Meanwhile, the factors affecting the ventilation rate were tested for significance, as presented in Figure 18b, with highly significant differences obtained for the variables at $p < 0.01$. Therefore, the main factors affecting the ventilation rate of greenhouses at high altitude are the inlet velocity and the temperature difference between the inside and outside of the greenhouse.

3.2.3. Ventilation Rate Equation Fitting and Prediction Validation

The calculation equation of the greenhouse ventilation rate in the high-altitude area was obtained by a fitting correction on the basis of research on the greenhouse ventilation

rate by previous scholars. Then, the verification of the prediction of the formula for the greenhouse ventilation rate in the high−altitude area was performed.

The previous scholars Sherman and Grimsrud derived the equation for calculating the greenhouse ventilation rate based on Bernoulli's equation, as in Equation (12) [32,33].

$$\phi_v = A\sqrt{\left(f_u^2 u^2 + f_{\Delta\Theta}^2 \Delta\Theta\right)} \tag{12}$$

where A is the surface area for the infiltration of the greenhouse; $\Delta\Theta$ is the difference between the inside and outside temperatures, and f_u (-) and $f_{\Delta\Theta}$ (m s^{-1} $K^{-1/2}$) are wind and temperature factors.

After adjusting parameters such as the radiation model, reference pressure, the heat source within the plant, and the air density, the ventilation rates of the greenhouse in the plain area were computed separately for different time periods. The equation for fitting the ventilation rate of the greenhouse in the high-altitude area (Q_1) and the ventilation rate of the greenhouse in the plain area (Q_2) are displayed in Equation (13), where the fitted ARE, RMSE, and R^2 are 3.8%, 1.63 m^3/sm and 0.9973, respectively, as shown in Figure 19.

$$Q_1 = 0.665 + 1.022Q_2 \tag{13}$$

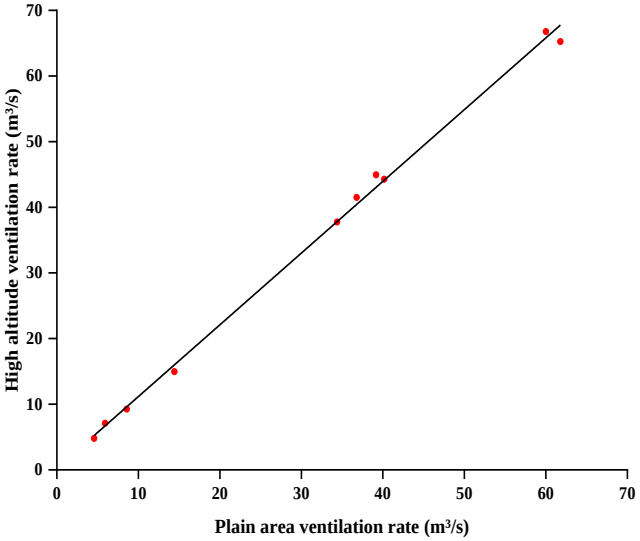

Figure 19. Fitted ventilation rate in the high-altitude area with the plain area ventilation rate.

Based on Equation (9), the multivariate nonlinear fit of the ventilation rate in the plain area results in f_u = 0.589 and $f_{\Delta\Theta}$ = 0.01 m s^{-1} $K^{-1/2}$. The ARE between the sample value and the fitted value is 4.55%, as shown in Figure 20.

The fitting formula for the plain area is substituted into Equation (10) to obtain the fitting formula for the greenhouse ventilation rate in the high-altitude area, as shown in Equation (11), where f_u = 0.589 and $f_{\Delta\Theta}$ = 0.01 m s^{-1} $K^{-1/2}$. The ARE, RMSE, and R^2 between the sample value and the fitted value are 4.55%, 0.543 m^3/s, and 0.9997, respectively, as displayed in Figure 21.

$$Q_1 = 0.665 + 1.022A\sqrt{\left(f_u^2 u^2 + f_{\Delta\Theta}^2 \Delta\Theta\right)} \tag{14}$$

The predictions of the winter (3 January 2022) greenhouse ventilation rate in high-altitude areas are shown in Figure 22. The ARE, RMSE, and R^2 of the prediction results are 9.726%, 8.435 m^3/s, and 0.9901, respectively, indicating that the accuracy is higher and the greenhouse ventilation rate can be better calculated in high-altitude areas.

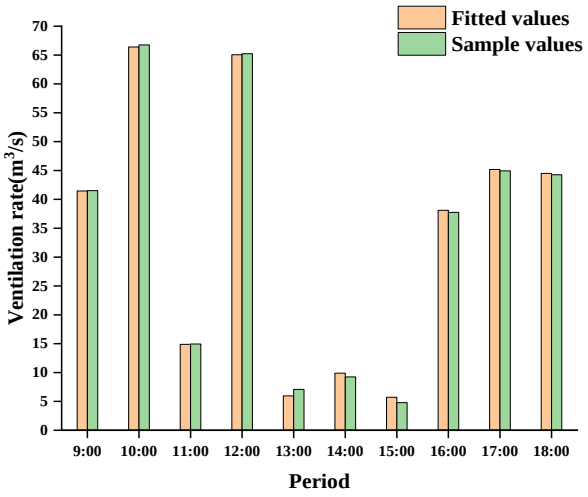

Figure 20. Comparison of calculated and fitted results before the correction of the ventilation rate in the plain area.

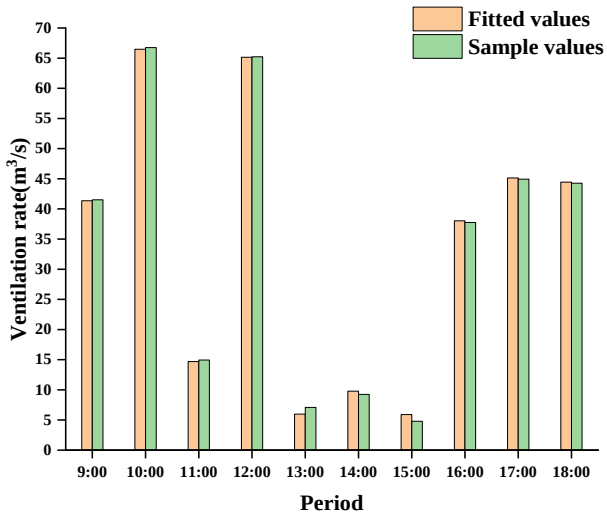

Figure 21. Comparison of the fitted and sample values in the high-altitude area.

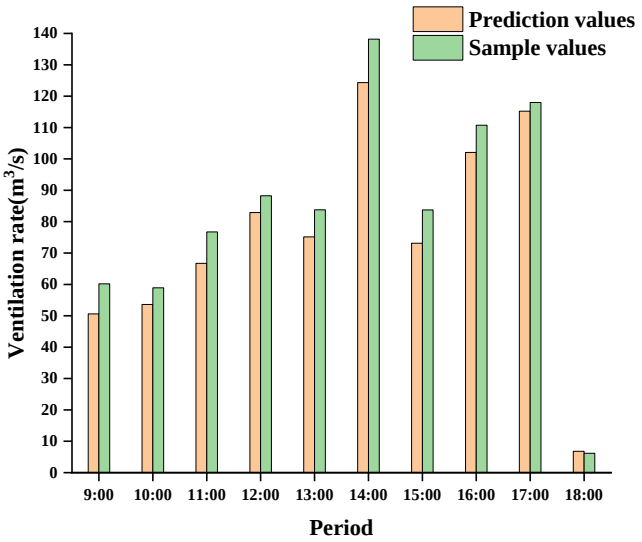

Figure 22. Comparison of predicted and sample values of the greenhouse ventilation rate in the high-altitude area.

4. Conclusions

A model of a solar greenhouse in a high-altitude region was constructed and verified based on the measured temperature and velocity using remote transmission and CFD technology.

The wind-induced and buoyancy-induced natural ventilation characteristics in greenhouses in both plain (altitude 43.5 m) and plateau (altitude 3650 m) areas were studied. The calculation results show that the wind velocity is relatively high (u = 1.95 m/s), so the wind pressure dominates the ventilation; the wind velocity is lower (u = 0.27 m/s), and the thermal pressure dominates the ventilation; and the wind velocity is increased (u = 1.3 m/s), and the wind pressure is coupled with the thermal pressure. In the greenhouse, the average values of wind pressure, Re, air density, and heat pressure in both the crop and non-crop sections are 75.91%, 46.2%, 66%, and 37.32% of those in the plain area, respectively.

The correlation coefficients of five relevant factors affecting the natural ventilation rate of the greenhouse in the high-altitude area were calculated for the inlet velocity (1.0), the temperature difference (−0.83) and air density difference (−0.72) between the inside and outside of the greenhouse, total indoor radiation (−0.72), and the internal heat source of the crop (0.68). In addition, the significance test resulted in two variables that were highly significant for the ventilation rate: the inlet velocity and the temperature difference between the inside and outside of the greenhouse.

A natural ventilation rate model for the plateau area was developed, with the ARE, RMSE, and R^2 between the sample values and the fitted values determined to be 4.55%, 0.543 m^3/s, and 0.9997, respectively. The model was validated by predicting the greenhouse ventilation rate in winter (3 January 2022), and the ARE, RMSE, and R^2 of the sample values and predicted values are 9.726%, 8.435 m^3/s, and 0.9901, respectively.

Author Contributions: Writing—original draft, B.L.; writing—review and editing, T.D.; supervision, S.Z.; project administration, Y.L.; data curation, P.W., Z.L. and J.Z. All authors have read and agreed to the published version of the manuscript.

Funding: This research was funded by the Natural Science Foundation of China (U20A2020) and the Beijing Vegetable Facility Industry System.

Data Availability Statement: Not applicable.

Conflicts of Interest: The authors declare no conflict of interest.

References

1. Wang, K. Environmental Simulation and Optimization of Multi-Span Plastic Greenhouse in Hainan. Master's Degree, Hainan University, Hainan, China, 2020.
2. Agarwal, A.; Gupta, S.; Ahmed, Z. Influence of plant densities on productivity of bell pepper (*Capsicum annuum* L.) under greenhouse in high altitude cold desert of Ladakh. In Proceedings of the International Symposium on Medicinal and Nutraceutical Plants 756, Macon, GA, USA, 19–23 March 2007; pp. 309–314.
3. Acharya, S.; Kumar, H. Effect of some organic manure on growth and yield of garlic in greenhouse condition at cold desert high altitude Ladakh Region. *Def. Life Sci. J.* **2018**, *3*, 100–104. [CrossRef]
4. Yin, C.; Pang, X.; Lei, Y. Populus from high altitude has more efficient protective mechanisms under water stress than from low-altitude habitats: A study in greenhouse for cuttings. *Physiol. Plant.* **2009**, *137*, 22–35. [CrossRef]
5. Fuller, R.; Aye, L.; Zahnd, A.; Thakuri, S. Thermal evaluation of a greenhouse in a remote high altitude area of Nepal. *Int. Energy J.* **2009**, *10*, 71–80.
6. Cheng, X.; Huang, Y.; Ren, H.; Ren, Z. Simulation of summer mechanical ventilation in flower greenhouses based on CFD. *J. Hebei Agric. Univ.* **2021**, *44*, 113–118. (In Chinese)
7. Liu, J.; Wen, X.; Li, Y.; Bai, J. Effect of the Wall of Solar Greenhouse with Forced Ventilation on the Indoor Temperature and Humidity. *J. Shanxi Agric. Sci.* **2018**, *46*, 421–425. (In Chinese)
8. Jerszurki, D.; Saadon, T.; Zhen, J.; Agam, N.; Tas, E.; Rachmilevitch, S.; Lazarovitch, N. Vertical microclimate heterogeneity and dew formation in semi-closed and naturally ventilated tomato greenhouses. *Sci. Hortic.* **2021**, *288*, 110271. [CrossRef]
9. Shen, M.; Hao, F. Numerical simulation of airflow distribution inside a tunnel greenhouse under two typical outside wind directions. *Nongye Gongcheng Xuebao* **2004**, *20*, 227–232.
10. Xu, F.; Cai, Y.; Chen, J.; Zhang, L. Temperature/flow field simulation and parameter optimal design for greenhouses with fan-pad evaporative cooling system. *Trans. Chin. Soc. Agric. Eng.* **2015**, *31*, 201–208.

11. Meneses, J.F.; Raposo, J.R. Ventilação natural de instalações agrícolas: Teoria e métodos de cálculo. *An. Inst. Super. Agron.* **1987**, *42*, 249.
12. Boulard, T.; Meneses, J.; Mermier, M.; Papadakis, G. The mechanisms involved in the natural ventilation of greenhouses. *Agric. For. Meteorol.* **1996**, *79*, 61–77. [CrossRef]
13. Boulard, T.; Papadakis, G.; Kittas, C.; Mermier, M. Air flow and associated sensible heat exchanges in a naturally ventilated greenhouse. *Agric. For. Meteorol.* **1997**, *88*, 111–119. [CrossRef]
14. Ge, J.; Xin, Q.; Gong, X.; Ping, Y.; Bo, G.; Li, Y. Effects of greenhouse ventilation and water control conditions on water consumption characteristics and yield of tomato. *J. Agric. Eng.* **2021**, *37*, 204–213. (In Chinese)
15. Okushima, L.; Sase, S.; Nara, M. A support system for natural ventilation design of greenhouses based on computational aerodynamics. In Proceedings of the International Symposium on Models for Plant Growth, Environmental Control and Farm Management in Protected Cultivation 248, Hanover, Germeny, 28 August–2 September 1988; pp. 129–136.
16. Mistriotis, A.; Bot, G.; Picuno, P.; Scarascia-Mugnozza, G. Analysis of the efficiency of greenhouse ventilation using computational fluid dynamics. *Agric. For. Meteorol.* **1997**, *85*, 217–228. [CrossRef]
17. Vollebregt, H.; Van de Braak, N. Analysis of radiative and convective heat exchange at greenhouse walls. *J. Agric. Eng. Res.* **1995**, *60*, 99–106. [CrossRef]
18. Cheng, X.; Mao, H.; Wu, D.; Li, B. Numerical simulation of thermal profiles in spatial and temporal field for natural ventilated glasshouse. *Trans. Chin. Soc. Agric. Mach.* **2009**, *40*, 179–183.
19. Kim, K.; Yoon, J.-Y.; Kwon, H.-J.; Han, J.-H.; Son, J.E.; Nam, S.-W.; Giacomelli, G.A.; Lee, I.-B. 3-D CFD analysis of relative humidity distribution in greenhouse with a fog cooling system and refrigerative dehumidifiers. *Biosyst. Eng.* **2008**, *100*, 245–255. [CrossRef]
20. Roy, J.; Fatnassi, H.; Boulard, T.; Pouillard, J.-B.; Grisey, A. CFD determination of the climate distribution in a semi closed greenhouse with air cooling. In Proceedings of the International Symposium on New Technologies and Management for Greenhouses-GreenSys2015 1170, Evora, Portugal, 19–23 July 2015; pp. 103–110.
21. Boulard, T.; Roy, J.-C.; Pouillard, J.-B.; Fatnassi, H.; Grisey, A. Modelling of micrometeorology, canopy transpiration and photosynthesis in a closed greenhouse using computational fluid dynamics. *Biosyst. Eng.* **2017**, *158*, 110–133. [CrossRef]
22. Boulard, T.; Roy, J.; Fatnassi, H.; Kichah, A.; Lee, I. Computer fluid dynamics prediction of climate and fungal spore transfer in a rose greenhouse. *Comput. Electron. Agric.* **2010**, *74*, 280–292. [CrossRef]
23. Akrami, M.; Javadi, A.A.; Hassanein, M.J.; Farmani, R.; Dibaj, M.; Tabor, G.R.; Negm, A. Study of the effects of vent configuration on mono-span greenhouse ventilation using computational fluid dynamics. *Sustainability* **2020**, *12*, 986. [CrossRef]
24. Hong, S.-W.; Lee, I.-B.; Hwang, H.-S.; Seo, I.-H.; Bitog, J.; Yoo, J.-I.; Kim, K.-S.; Lee, S.-H.; Kim, K.-W.; Yoon, N.-K. Numerical simulation of ventilation efficiencies of naturally ventilated multi-span greenhouses in Korea. *Trans. ASABE* **2008**, *51*, 1417–1432. [CrossRef]
25. Li, H.; Ji, D.; Hu, X.; Xie, T.; Song, W.; Tian, S. Comprehensive evaluation of combining CFD simulation and entropy weight to predict natural ventilation strategy in a sliding cover solar greenhouse. *Int. J. Agric. Biol. Eng.* **2021**, *14*, 213–221. [CrossRef]
26. He, K.; Chen, D.; Sun, L.; Liu, Z. Effects of Wind Regime and Vent Configuration on Microclimate in Tunnel Greenhouses in Summer. *J. Agric. Mach.* **2017**, *48*, 311–339.
27. Boulard, T.; Baille, A. Modelling of air exchange rate in a greenhouse equipped with continuous roof vents. *J. Agric. Eng. Res.* **1995**, *61*, 37–47. (In Chinese) [CrossRef]
28. Baptista, F.; Bailey, B.; Randall, J.; Meneses, J. Greenhouse ventilation rate: Theory and measurement with tracer gas techniques. *J. Agric. Eng. Res.* **1999**, *72*, 363–374. [CrossRef]
29. Fang, H.; Yang, Q.; Zhang, Y.; Cheng, R.; Zhang, F.; Lu, W. Simulation on ventilation flux of solar greenhouse based on the coupling between stack and wind effects. *Chin. J. Agrometeorol.* **2016**, *37*, 531.
30. Kittas, C.; Boulard, T.; Papadakis, G. Natural ventilation of a greenhouse with ridge and side openings: Sensitivity to temperature and wind effects. *Trans. ASAE* **1997**, *40*, 415–425. [CrossRef]
31. Wang, L.; Zhou, C. Determination of calculated method for necessary ventilation rate and its determination analysis of parameter value. *Trans. Chin. Soc. Agric. Eng.* **2017**, *33*, 190–198.
32. Sherman, M.H. Infiltration-Pressurization Correlation: Simplified Physical Modeling. 1980. Available online: https://www.osti.gov/biblio/5443198 (accessed on 29 September 2022).
33. Fernandez, J.; Bailey, B. Measurement and prediction of greenhouse ventilation rates. *Agric. For. Meteorol.* **1992**, *58*, 229–245. [CrossRef]
34. Wu, F.; Xu, F.; Zhang, L.; Ma, X. Numerical simulation on thermal environment of heated glass greenhouse based on porous medium. *Trans. Chin. Soc. Agric. Mach.* **2011**, *42*, 180–185.
35. Jiang, G.; Hu, Y.; Liu, Y.; Zou, Z. Analysis on insulation performance of sunken solar greenhouse based on CFD. *Trans. Chin. Soc. Agric. Eng.* **2011**, *27*, 275–281.
36. Jain, D.; Tiwari, G.N. Modeling and optimal design of evaporative cooling system in controlled environment greenhouse. *Energy Convers. Manag.* **2002**, *43*, 2235–2250. [CrossRef]
37. Miao, Z. Numerical Simulation and Optimization of Vent Configuration for Natural Ventilation of the Large Space Exhibition Greenhouse. *Refrig. Air Cond.* **2020**, *34*, 29–38. (In Chinese)

38. Wei, J. Research on Experimental and Simulation of Soil-Crop-Environment Hydrothermal System in Typical Double-Flim Solar Greenhouse in Cold and Arid Regions. Ph.D. Thesis, Inner Mongolia Agricultural University, Hohhot, China, 2021.
39. Luan, Z.; Zhou, Z.; Huang, S.; Ye, M. Investigation on the effect of buoyancy on the subcooled flow boiling heat transfer characteristics of water in tubes. *Nucl. Fusion Plasma Phys. PKU* **2022**, *42*, 236–243. (In Chinese)
40. Luo, T. *Fluid Mechanics*; Mechanical Engineering Press: Beijing, China, 2017.
41. Zhang, Y.; Henke, M.; Li, Y.; Yue, X.; Xu, D.; Liu, X.; Li, T. High resolution 3D simulation of light climate and thermal performance of a solar greenhouse model under tomato canopy structure. *Renew. Energy* **2020**, *160*, 730–745. [CrossRef]
42. Chen, N.; Liao, S.; Rao, Z. Numerical investigation of heat and mass transfer in hypobaric atmosphere. *J. Cent. South Univ.* **2013**, *44*, 388–396.
43. Shklyar, A.; Arbel, A. Numerical model of the three-dimensional isothermal flow patterns and mass fluxes in a pitched-roof greenhouse. *J. Wind Eng. Ind. Aerodyn.* **2004**, *92*, 1039–1059. [CrossRef]